Experimental verification of source-mask optimization and freeform illumination for 22-nm node static random access memory cells

Joost Bekaert
Bart Laenens
Staf Verhaegen
Lieve Van Look
Darko Trivkovic
Frederic Lazzarino
Geert Vandenberghe
Imec vzw
Kapeldreef 75
3001 Leuven, Belgium
E-mail: joost.bekaert@imec.be

Paul van Adrichem
ASML-BRION
4210 Burton Drive
Santa Clara, California 95054
and
ASML
De Run 6501
5504 DR Veldhoven, The Netherlands

Robert Socha
Stephen Hsu
Hua-Yu Liu
ASML-BRION
4210 Burton Drive
Santa Clara, California 95054

Orion Mouraille
Koen Schreel
Mircea Dusa
ASML
De Run 6501
5504 DR Veldhoven, The Netherlands

Jörg Zimmermann
Paul Gräupner
Jens Timo Neumann
Carl Zeiss SMT AG
73446 Oberkochen, Germany

Abstract. The use of customized illumination modes is part of the pursuit to stretch the applicability of immersion ArF lithography. Indeed, a specific illumination source shape that is optimized for a particular design leads to enhanced imaging results. Recently, freeform illumination has become available through pixelated diffractive optical elements or through ASML's programmable illuminator system (FlexRay^{TM}) allowing for virtually unconstrained intensity distribution within the source pupil. In this paper, the benefit of freeform over traditional illumination is evaluated, by applying source mask co-optimization (SMO) for an aggressive use case and wafer-based verification. For a 22-nm node SRAM of 0.099 and 0.078 μm^2 bit cell area, the patterning of the full contact and metal layer into a hard mask is demonstrated with the application of SMO and freeform illumination. In this work, both pixelated diffractive optical elements and FlexRay are applied. Additionally, the match between the latter two is confirmed on wafer, in terms of critical dimension and process window. © *2011 Society of Photo-Optical Instrumentation Engineers (SPIE).* [DOI: 10.1117/1.3541778]

Subject terms: source mask co-optimization, FlexRay; source mask optimization; freeform illumination; static random access memory, negative tone development.

Paper 10026PR received Apr. 2, 2010; revised manuscript received Oct. 13, 2010; accepted for publication Dec. 8, 2010; published online Mar. 10, 2011.

1 Introduction

1.1 *Extending the Reach of ArF Lithography*

Lithographic research and development has reached a very interesting stage. The physical limit of water-based immersion ArF lithography has been attained with the accomplishment of full-field scanners with a numerical aperture (NA) of 1.35. Such systems have nowadays found their place in the production flow of all advanced integrated circuit (IC) manufacturers.

1932-5150/2011/$25.00 © 2011 SPIE

The gap that developed between the current optical lithography and its expected successors needs to be filled up. In this, double patterning techniques play the leading role, even though they may turn out to be costly solutions for a couple of nodes only. In view of this, a lot of effort is spent to stretch ArF immersion lithography at 1.35 NA to its application limits; e.g., double exposure schemes, litho-friendly design, alternative processing schemes using novel materials, . . . etc. Also, customized illumination modes are applied to improve the patterning fidelity for specific designs. Moreover, any stretching of the single patterning limits eventually implies stretching of the double patterning limits.

Downloaded From: http://nanolithography.spiedigitallibrary.org/ on 04/08/2013 Terms of Use: http://spiedl.org/terms

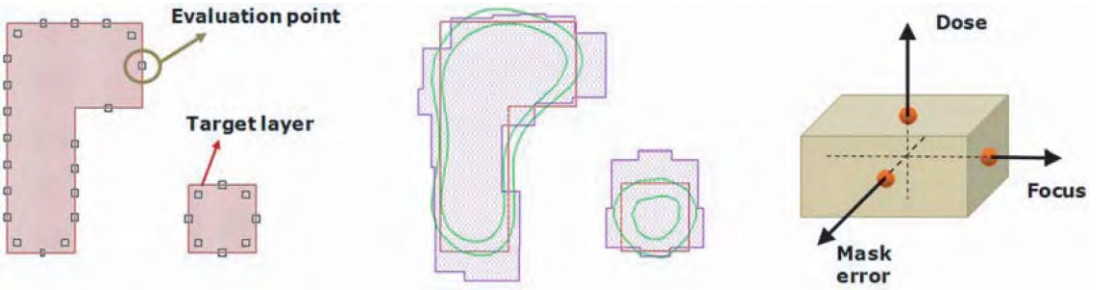

Fig. 1 Illustration of target layer and evaluation points around the contour. In ASML BRION Tachyon SMO, the weighted edge placement error is minimized within user-specified dose, focus, and mask error conditions.

1.2 *Source Mask Optimization and Freeform Illumination*

The work presented here is to be seen in the light of customized illumination types. In an experimental manner, it focuses on the application of simultaneous source and mask co-optimization (SMO). In SMO, the input is basically a given clip containing the target design, and the output of the optimization consists of an illumination source shape together with a clip containing the corresponding optical proximity correction (OPC). As such, a routine for source optimization is not new, but the novelty mainly lies in the co-optimization of the mask, and the output of "freeform" sources.[1–6]

In freeform illumination, there is basically unlimited freedom in intensity and position of the light in the illumination pupil. In practice, a freeform source is often pixelated, with free choice of intensity per pixel, and smoothened by a point spread function. Similar to the traditional standard source shapes (e.g., Quasar, CQuad, Annular), freeform illumination shapes can be achieved on scanners using diffractive optical elements (DOE), which create one particular source shape.[7,8] Additionally, a programmable illuminator called FlexRay^{TM} is presented on ASML scanners as an option that allows instantaneous and unlimited variations of source shape set-up.[7,9–11]

The final goal of the SMO and freeform illumination technique is first to increase the yield of the lithographic process, e.g., through increase in process latitude or mask error enhancement factor (MEEF). In addition, the technique can create a margin that allows for further downscaling of the device.

In this paper, we go through the full SMO flow; starting from an aggressive use case, over the SMO optimization and actual creation of source and mask, to experimental validation on wafer with both DOE and FlexRay illumination. More in particular, the benefit of using a freeform source over a traditional (standard) source shape is studied for a 22 nm node static random access memory (SRAM) pattern. This benefit of freeform over standard sources, or any potential drawback, is evaluated for different metrics such as exposure latitude (EL), depth of focus (DoF), MEEF, but an assessment is also made concerning critical dimension (CD) uniformity, lens heating characteristics, . . . etc.

2 Source Mask Optimization with ASML Brion Tachyon SMO

ASML BRION Tachyon SMO^{TM} simultaneously co-optimizes the scanner source and mask to achieve the best possible process window and to ensure manufacturability. Co-optimization of the illuminator and mask has great advantage over an iterative approach in finding the best solution under the manufacturability constraints. Tachyon SMO includes the available illumination conditions for ASML's advanced scanner platforms. It also uses the most advanced illumination predictive models for standard, custom, and freeform sources to ensure that manufacturable solutions are found with the most accurate analysis available.

Tachyon SMO uses an intuitive cost function (*CF*) that is based on through-process edge placement error (EPE)

$$CF = \sum_{pw} \sum_{x} W(pw, x).||EPE(pw, x)||^{p}. \quad (1)$$

The EPE is the CD difference between the predicted resist contour and the target design, evaluated at user-defined evaluation points (demonstrated in Fig. 1). The cost function, which is to be minimized, sums the EPE^{p} over all evaluation points (x) around the target contours and user-defined process window (pw) conditions. The process window conditions considered in Tachyon SMO include Δdose, defocus, and mask error, which equivalently optimizes exposure EL, DoF, and MEEF. The variable p is the power over the EPE. The factor W is a weight factor to provide extra flexibility to adjust the relative significance of different sampling points. This formulation essentially minimizes the maximum EPE across all evaluation points and all process window conditions.[5,6]

The first step in the SMO flow is for the user to set up all input parameters for the optimization, including resist model, source type (freeform, parametric, or standard types shown in Fig. 2), minimal source fill factor, polarization condition, mask type and structure, mask manufacturability rule check (MRC constraints), and process information. Also, the

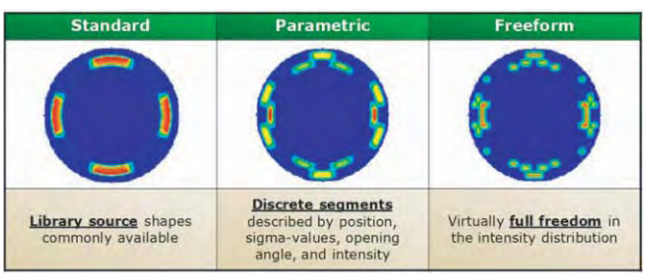

Fig. 2 Description and example of a standard, parametric, and freeform source type. These are the illumination choices for optimization in ASML BRION Tachyon SMO.

Downloaded From: http://nanolithography.spiedigitallibrary.org/ on 04/08/2013 Terms of Use: http://spiedl.org/terms

user places the evaluation points at physically reasonable locations. With all the setup parameters, the optimization starts with an unconstrained freeform source and a continuous transmission mask. Without constraints, optimization in this stage will search for solutions in the largest possible solution space and give the best possible process window and MEEF. However, neither the unconstrained source nor the continuous transmission mask is manufacturable. Therefore, in the next step the source is converted into a manufacturable source such as a source generated by a DOE. On the mask side, the transmission is constrained to a fixed value and assist features are extracted from the mask gray tone image. Then, in the final step, the constrained source along with the main and assist features on the mask are optimized taking the scanner illuminator and the MRC constraints into account.[5,6]

After the optimization, the user can obtain and analyze the process window and MEEF results at user-defined positions, and process variation bands can be evaluated.

3 Increasing Yield: Freedom versus Standard Source for the Contact Layer of an 0.099 μm^2 SRAM Cell

3.1 *SMO Result: Optimized Freeform and Standard Source, and Verification of DOE-based Freeform Source*

In the SMO exercise, and hence in the subsequent experiments, the input settings are the following:

Layout clip. The case under investigation is the contact layer of a 22 nm node SRAM, with 0.099 μm^2 bit cell area. The pattern is depicted in the left image of Fig. 3. It has minimum pitch 110 nm in X (horizontal) and 90 nm in Y (vertical, $k_1 = 0.314$). With or without SMO, this is far too dense for single patterning with adequate process latitudes, so the pattern has been split for double patterning (DP). The split is done in such a way that the two split patterns are equal, but shifted with respect to each other (blue and yellow pattern in Fig. 3). In this way, the SMO solution found for the first split pattern is the same as that for the second split pattern, which means that the same source can be used for both. After DP split, the minimum pitch is still 110 nm in X ($k_1 = 0.384$) but 180 nm in Y.

The pattern has an XY mirror symmetry of the bit cell, such that 2×2 bit cells jointly form the unit cell of the pattern (shown in Fig. 3). The target size of the contacts after litho was chosen to be 54 nm and 104 nm $\times$ 54 nm for the elongated contacts.

Wafer and resist stack. Both in the source-mask simulation as in the actual wafer experiments, a representative back-end wafer stack was chosen consisting of a TiN hard mask (HM) layer on top of a thick dielectric oxide layer. The resist stack on top of the HM consists of a 35 nm bottom anti-reflective coating (Brewer/Nissan ARC160) and a 100 nm thick resist layer (FujiFilm FAIRS9101-A19C). A calibrated resist model was not yet available for the selected resist. Therefore, for the source optimizations and the OPC performed in the SMO in this work, a resist model based on a 12 nm optical blur setting was used as a best-guess approximation.

After investigation of a variety of options, it was found that the better results were predicted using the following settings:

Negative tone development. It has been demonstrated how the use of a light field mask with dots at the contact positions in combination with the application of negative tone development (NTD) leads to improved contact patterning.[12,13] This was confirmed in the SMO runs for the particular contact case in this study. NTD is an image reversal technique for positive tone resists, in which the unexposed ("dark") resist dissolves in a solvent-based developer product (FujiFilm), while the

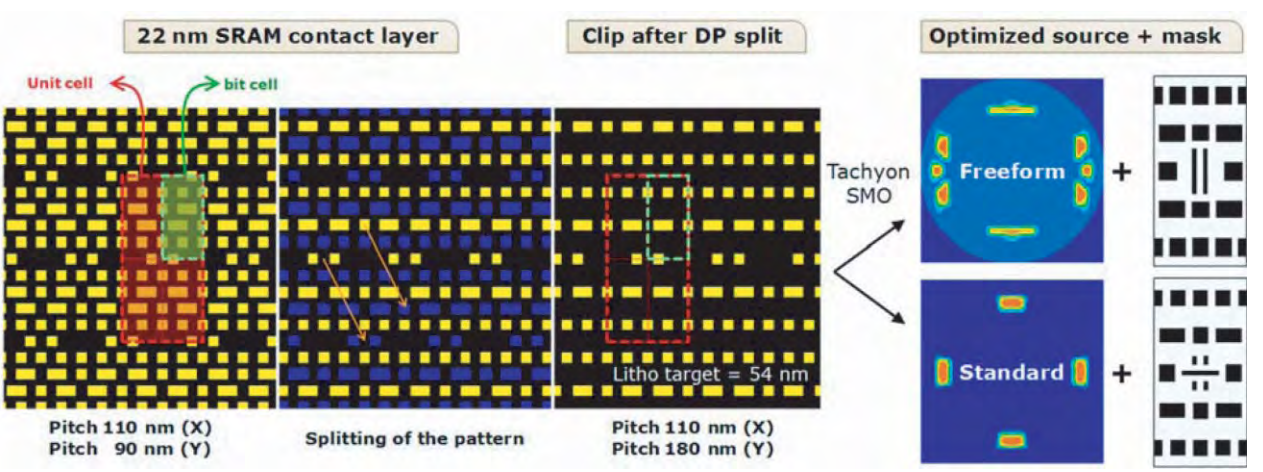

Fig. 3 Input and output of the SMO calculation. On the left: three patterns respectively showing the full SRAM contact layer, the splitting of the layer for double patterning, and the clip after split as used for the SMO calculations. The unit cell (indicated in red) consists of 4 bit cells (indicated in green). The orange arrows indicate the shift over which the two split patterns are identical. On the right: the optimized freeform and standard sources are shown together with their respective optimized mask (OPC + assist features). With the application of negative tone development, the mask is a light field mask with dots at the contact positions. (Color online only.)

Downloaded From: http://nanolithography.spiedigitallibrary.org/ on 04/08/2013 Terms of Use: http://spiedl.org/terms

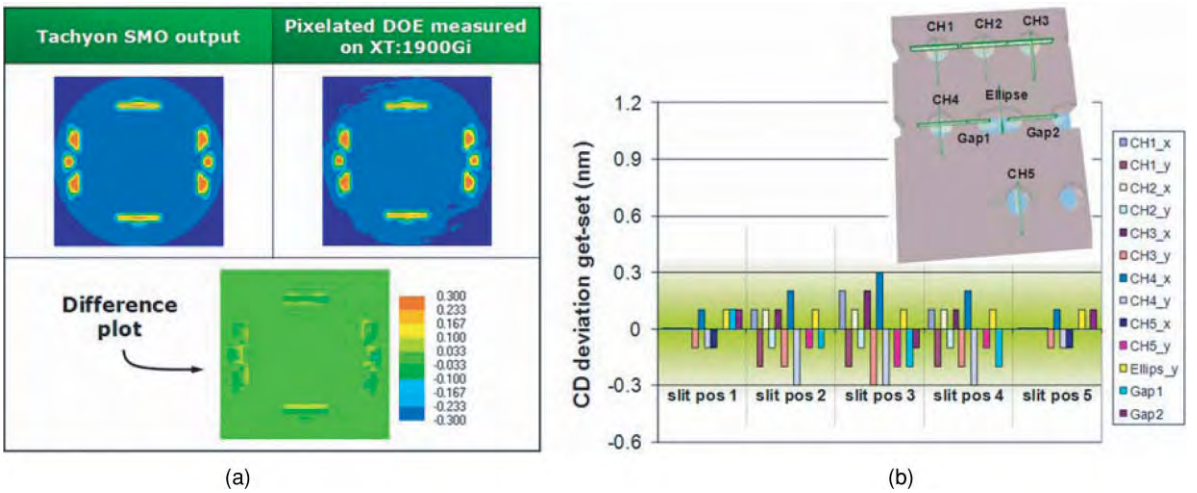

Fig. 4 Verification of the manufactured freeform source (based on pixelated DOE). (a) Target source from Tachyon SMO compared to measured source on ASML TWINSCAN XT:1900i. (b) KLA Prolith simulation result showing impact on the CD for the contact features in the SRAM clip (difference after subtracting the CDs obtained with the measured source from those obtained with the target source).

exposed resist remains. By applying this technique for contacts patterning, the use of a light field mask (as shown in Fig. 3 above) leads to an improved optical image as compared to the traditional approach of dark field contact masks and standard (positive) development.

A standard 6% attenuated phase shift mask was selected, as the modeled result after SMO appeared slightly better than for a binary mask. Also, selecting XY polarization for the source predicted the better result compared to X, Y, or unpolarized light. The numerical aperture was set to 1.35 NA, being the limit for water-based immersion, and the maximal NA that can be reached by the scanners used in this work.

For further experimental comparison, the freeform and standard source types were selected in the source optimization. In order to ensure a fair comparison of these two cases in terms of the conditions of generation of the SMO mask and source, all input parameters were kept equal when performing the calculations for freeform and standard source. The output result of the Tachyon SMO is shown at the right side in Fig. 3. The optimized mask consists of the SRAM clip's unit cell treated with OPC and assist features. As optimal standard source for the given clip, the SMO proposed a CQuad setting (CQuad 20°, Sigma settings 0.815-0.688).

Next, a freeform "pixelated" DOE was manufactured based on the SMO output freeform source. After installation of the DOE into an ASML XT:1900i scanner, the obtained freeform source pupil was measured and compared to the given target source. The result is shown in Fig. 4. In the image on the left side of Fig. 4, it is shown that the match between measured ("get") and target ("set") source is extremely good. In particular when considering the difference pupil, it can be seen that maximal deviations from target are no more than ∼15% of the peak intensity, and this on very small pupil areas. In common cases, source pupil differences can further be reduced by a dedicated pupil calibration to fine-tune, e.g., zoom and beam centering. The latter was not carried out in this work, as the delta-pupil was minimal to start from. Instead, a simulation (KLA Prolith) was made of the impact on CD due to any difference between the measured source and the SMO output target source. The result is shown in the graph at the right side of Fig. 4. For 13 different cut-lines within the SRAM bit cell, the CD difference is derived from the CDs obtained using the individual sources. Even with the freeform source measured in five positions through the exposure slit, the simulated impact on the CD is less than 0.3 nm for all cut-lines, proving excellent DOE manufacturability and scanner set-up. Also, it confirms that the Tachyon SMO correctly takes the source manufacturing constraints into account.

3.2 *Freeform versus Standard Source: Wafer-based Comparison of Process Latitudes and MEEF*

Besides the manufacturing and installation of the freeform DOE, the standard CQuad source was also installed on the same ASML XT:1900i. Next, a dedicated mask was manufactured containing OPC'ed SRAM arrays created from the output of the Tachyon SMO. In addition to these "nominal" clips for the freeform and standard source, copies of the clips were added with small steps in global post-OPC bias, allowing for accurate MEEF determination after patterning on wafer.

First, the printing of the pattern on wafer is confirmed: the left scanning electron microscope (SEM) image in Fig. 5 is obtained at best focus and best dose for the SRAM contact layer, after exposure with the freeform source. The resist model used during the SMO was simply an aerial image blur model. Nevertheless, the contacts were printed close to their target of 54 nm. After the patterning of the contacts into the resist layer, etch tests have been carried out to demonstrate the capability of pattern transfer into the TiN hard mask. Although no dedicated etch optimization was performed for the given case (mask, pattern, wafer and resist stack, . . . etc.), it could be shown that the split SRAM contact layer can be opened into the hard mask (P110/P180). Moreover, after a second litho and etch step using the same source and mask, the full contact layer could be reconstructed (P110/P90, right image in

Downloaded From: http://nanolithography.spiedigitallibrary.org/ on 04/08/2013 Terms of Use: http://spiedl.org/terms

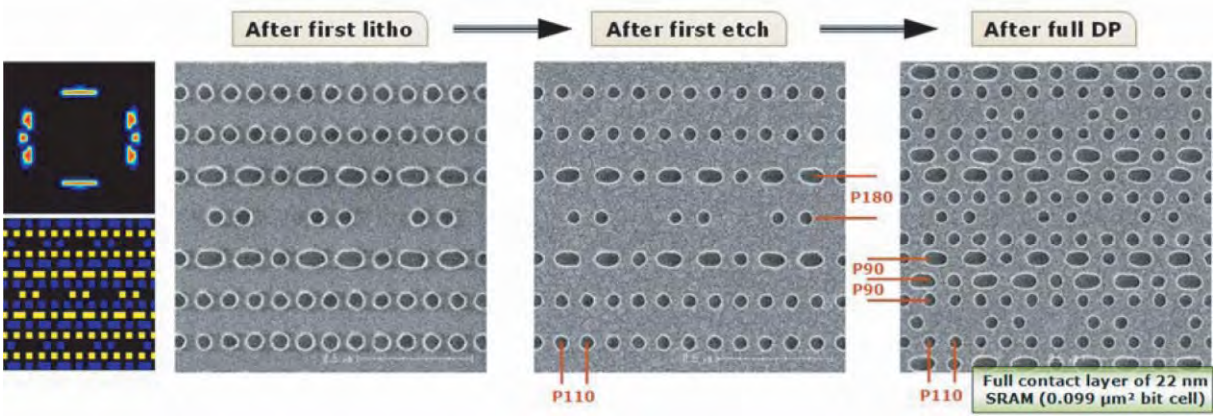

Fig. 5 DOE freeform source measured on an ASML XT:1900i, and SRAM contact target pattern (first litho yellow, second litho blue, see Fig. 3). SEM images: pattern in resist after first litho, after first etch into TiN hard mask, and after full double patterning (litho-etch-litho-etch). Initial result: nonoptimized etch process and alignment. (Color online only.)

Fig. 5). It must be noted that a basic alignment routine and no overlay correction was applied on the scanner, such that a minor overlay error resulted between the first and second patterning step.

Next, the process window and MEEF differences between the freeform and standard illumination cases are evaluated (after litho). To do so, the contact features are labeled based on symmetry, as is shown in Fig. 6, and measured using image-based metrology on a Hitachi CD-SEM (CG4000). The EL, DoF, and MEEF for the six different features are reported in the graphs of Fig. 6. On the target of 54/104 nm, a CD spec of ± 4 nm was applied.

In general, some increase in EL and DoF, and some decrease of MEEF, is observed for the case of the freeform source. Often, the improvement per individual metric is only moderate (e.g., 10–15%). However, when considering the combined gain over the different metrics, these individual benefits multiply to a considerable level (e.g., 30–50%).

Another way to consider the obtained results is by looking at the worst case numbers of each of the individual metrics. In this respect, it can be seen that the lowest EL among all measured features was improved from 5.3 to 7.4% by applying freeform illumination. Similarly, the lowest DoF was improved from 74 to 89 nm, and the highest MEEF was reduced from 4.4 to 4.1. These improvements are indicated by the dashed lines and arrows in Fig. 6.

Yet another relevant way to evaluate these results is by looking at the worst performing feature under the condition

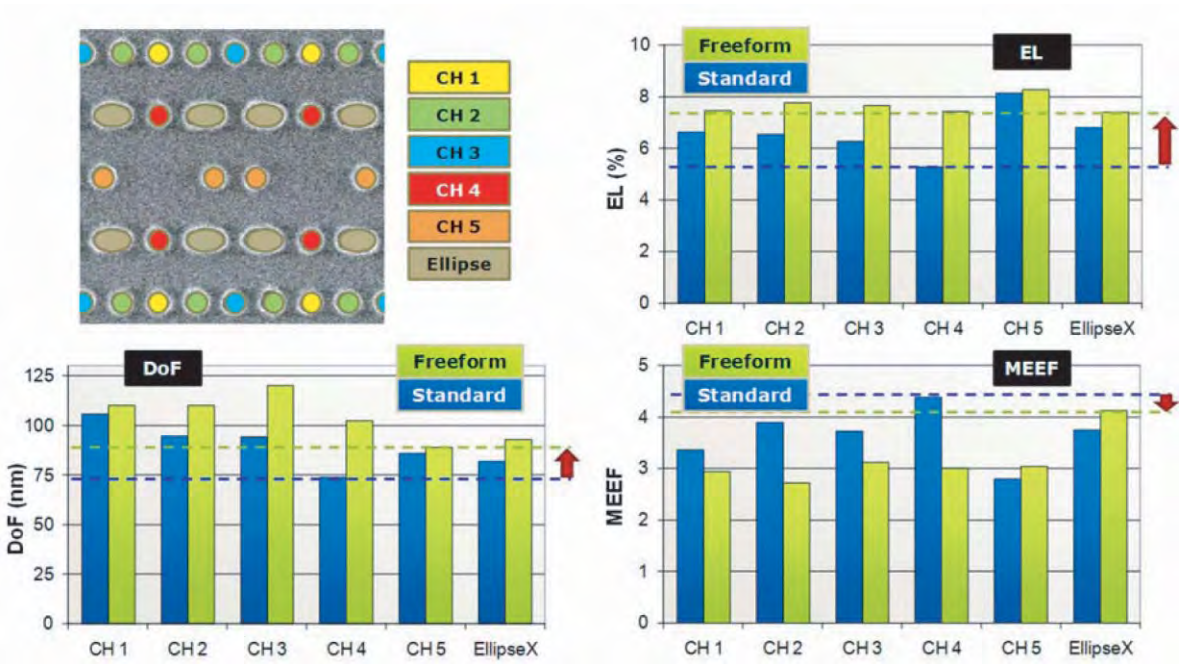

Fig. 6 Measurement results for EL, DoF, and MEEF demonstrating the benefit of freeform over standard source illumination. The data is shown for all different features in the contact clip, as defined in the upper-left image. The dashed lines and red arrows indicate the improvement of the lowest EL, lowest DoF, and highest MEEF. (Color online only.)

Downloaded From: http://nanolithography.spiedigitallibrary.org/ on 04/08/2013 Terms of Use: http://spiedl.org/terms

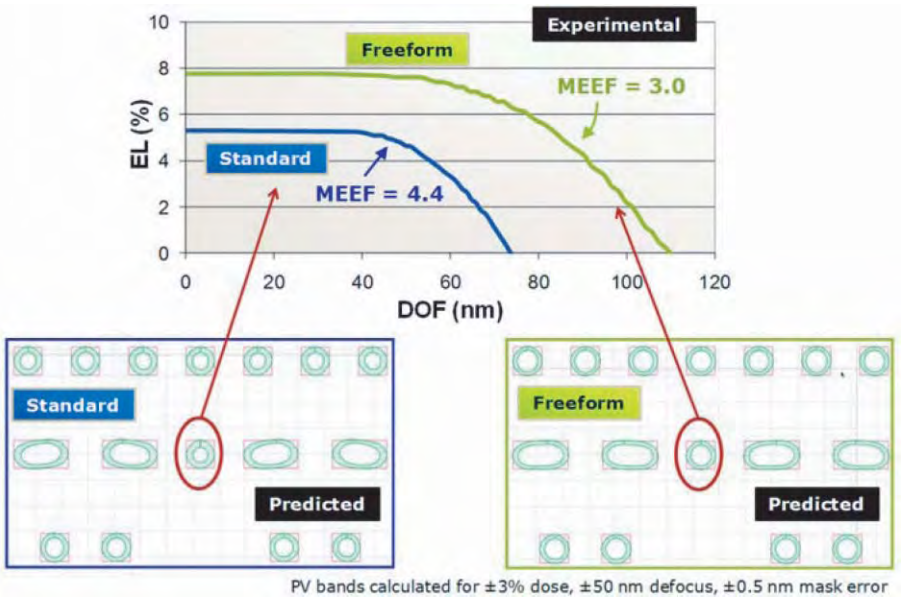

Fig. 7 Bottom: Tachyon SMO process variation band calculations for standard and freeform illumination, predicting a particular improvement for the contact in between the elongated contacts. Top graph: Experimental confirmation showing enhancement in process window and MEEF for the contact in between the elongated contacts (hotspot).

of standard illumination. This "hotspot" feature (CH_4) is the contact located in between the elongated contacts. Indeed, from the graphs it can be seen that this is the feature with lowest EL and DoF, and also the highest MEEF. The particular improvement for this feature is depicted in Fig. 7, clearly showing a large increase in process window area combined with good improvement in MEEF, resulting in a relief of the hotspot status of this feature. Figure 7 also shows a comparison of process variations (PV) bands, as modeled by the Tachyon SMO after the optimization of source and mask for both the freeform and standard source cases. A close look at these PV bands shows a pronounced improvement for the contact in between the elongated contacts, in line with the experimental findings.

The above results confirm the benefit of applying freeform illumination for the considered case.

3.3 *Freeform versus Standard Source: Wafer-based Comparison of CD Uniformity*

In addition to process window and MEEF, an assessment of the CD uniformity (CDU) has been included in the comparison of freeform versus standard illumination. Both for freeform and standard, a uniform wafer was exposed at best focus/dose condition. On each wafer, three dies with 56 subfields with 12 positions of 17 contacts were measured, from which the 3sigma CDU values were calculated for each feature defined in Fig. 6 above. Next, the CDU ratios for freeform over standard were calculated. From this ratio, the relative improvement in the CDU is derived.

The formula for the applied metric and obtained results are shown in Fig. 8. It demonstrates how, for the case in our study, freeform illumination improves the CDU for all features, on average by 17% and even up to 25% for CH_4

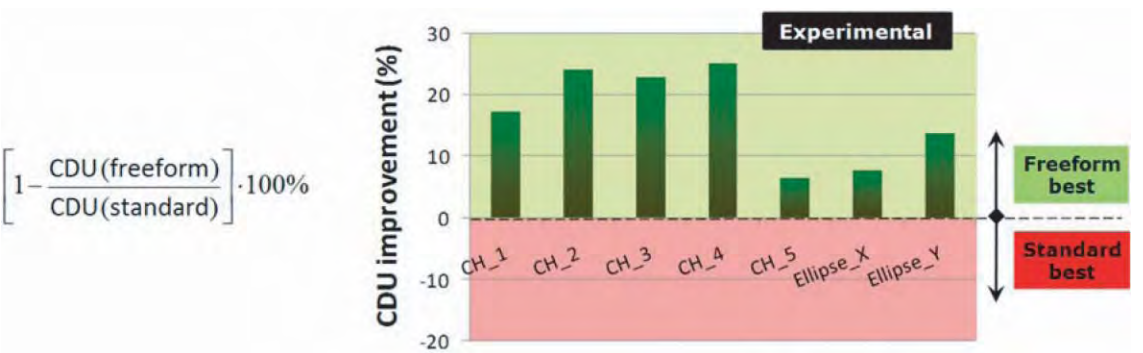

Fig. 8 Experimentally obtained CDU improvement for freeform over standard illumination, per feature in the SRAM contact clip (see Fig. 6). The formula defines the metric that was applied.

Downloaded From: http://nanolithography.spiedigitallibrary.org/ on 04/08/2013 Terms of Use: http://spiedl.org/terms

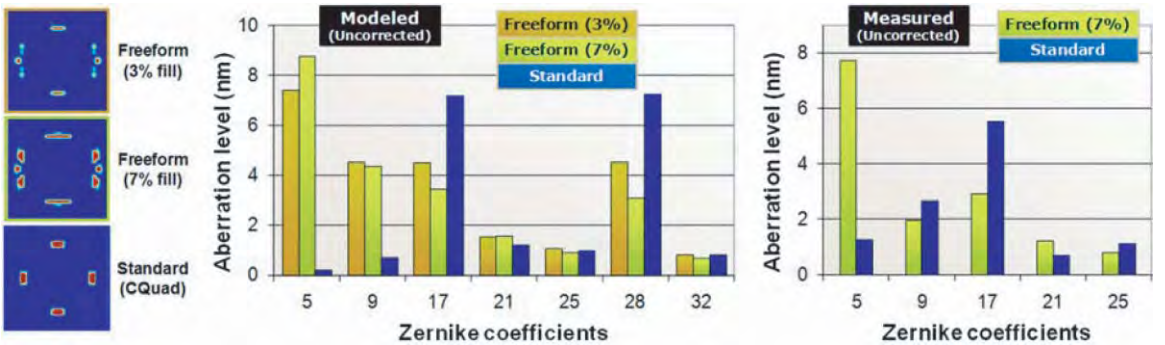

Fig. 9 Modeled and measured aberration levels before application of any lens heating correction, comparing freeform and standard sources. Only aberrations larger than 1 nm are shown. Two different pupil fill factors are considered for the freeform modeled results.

(contact in between the elongated contacts). The latter is the same feature that showed the largest improvement also in process window and MEEF (demonstrated in Fig. 7 above).

Control of the CDU is of ever increasing importance for the most advanced (including double patterning) applications.[14] Therefore, every potential contributor to CD variations over the wafer is subject to very tight specs, i.e., on scanner, reticle, or processing side. Similarly, every technique that can create improvement in the CDU is much appreciated. In a very direct manner, the outcome of this experiment demonstrates how SMO and freeform illumination clearly help in obtaining better CD control within the chips and thereby increase the yield of the production process.

3.4 *Freeform versus Standard Source: Comparison Lens Heating Characteristics*

Since the freeform pupil shapes may strongly differ from the traditional ones, they will accordingly lead to different lens heating signatures. Therefore, the concern may be raised as to whether the application of freeform sources would not lead to issues related to existing lens heating correction strategies.

For the SRAM contact case as presented above, the hot-state uncorrected aberrations have been determined and compared for both the freeform and standard source shape (under identical heat load). The aberrations, decomposed into Zernike polynomials, were obtained through modeling (based on source map, mask design, and lens specific information) but they were also measured from the scanner as part of the traditional lens heating correction calibration.

The modeled aberrations (>1 nm) are shown on the left graph of Fig. 9. In fact, the freeform result shown in that graph is obtained using two sources with different pupil fill factor, namely 3 and 7%, in order to evaluate its impact. The measured aberrations (>1 nm) are shown in the right graph. Note that these are aberration levels for a light field mask, before any application of lens heating correction.

In this assessment, the modeled and measured results lead to the following main conclusions for the case of this study:

> The aberrations induced by the freeform source are not particularly higher. They can equally well and in the same manner be corrected for as those originating from a standard source. In other words, the traditional lens heating compensation strategies are equally effective for freeform sources.
>
> Freeform sources naturally lead to another distribution of the aberrations, but do not necessarily lead to particularly increased aberration levels compared to standard sources. In the given example, the XY symmetric CQuad source triggers the 4-foil aberrations like Z17 and leaves astigmatism Z5 close to zero level, while the freeform source leads to more pronounced astigmatism and less 4-foil because of its different symmetry in X versus Y.
>
> For the given case, the impact of a lower fill factor is a minimal shift of the aberrations to higher orders.

4 Further Downscaling: Contact and Metal Layer of an 0.078 μm^2 SRAM Cell

In the following, the same SRAM contact clip is taken as above in Sec. 3, with a matching metal 1 layer, and downscaled by 20% to 0.078 μm^2 bit cell area. To achieve this, the minimum pitch in the X direction was reduced from 110 to 100 nm, and the minimum pitch in the Y direction was reduced from 90 to 78 nm (respectively from 180 to 156 nm after split for double patterning).

Exposures were performed on an ASML XT:1950i scanner equipped with a FlexRay illuminator. In Fig. 10, SEM images at best focus and dose are compared, obtained with the optimized freeform and standard sources for this downscaled contact case. The measured lowest EL and DoF, and highest MEEF among all features are reported for both illumination types. Already from the images, but in particular from the metrics, it is very clear how freeform illumination leads to a pattern quality that cannot be realized using standard illumination. In this particular case, the XY asymmetric position of the freeform poles cannot be mimicked in a standard source (this case: CQuad20°, σ 0.934–0.781).

Similar as for the 0.099 μm^2 SRAM above, the full double patterning for the 0.078 μm^2 SRAM is demonstrated in Fig. 11. It shows the contact and metal layer opened into a TiN hard mask, though with limited etch or overlay optimization.

Such SRAM with 0.078 μm^2 bit cell area is very advanced for ArF imaging, and may be somewhat over-aggressive in the sense that low contrast, low DoF, and high MEEF put tremendous demands on the scanner control (focus and dose, dynamics, etc.), on the mask (OPC correctness, reticle manufacturing: feature size and uniformity), and also on the resist process (edge roughness, uniformity, etc.). Therefore,

Downloaded From: http://nanolithography.spiedigitallibrary.org/ on 04/08/2013 Terms of Use: http://spiedl.org/terms

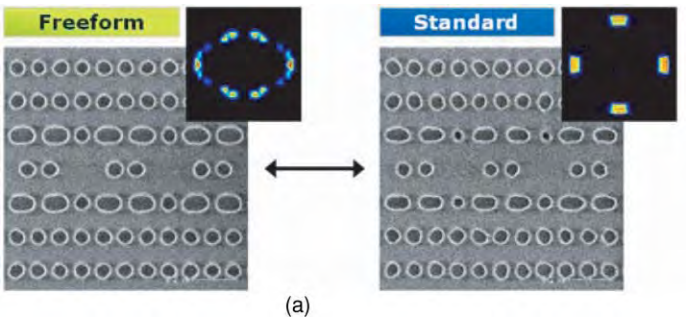

	Standard	Freeform
Lowest EL (%)	3.0	7.1
Lowest DOF (nm)	65	97
Max. MEEF	9.1	6.4

(b)

Fig. 10 Freeform versus standard illumination comparison for an 0.078 μm^2 SRAM contact layer (split for DP), exposed on an ASML XT:1950i with FlexRay illuminator. (a) SEM images at best focus and dose. (b) Measured worst case EL, DoF, and MEEF. The target in resist is 50 nm with a spec of ± 4 nm.

the best CD control and uniformity over the wafer can only be achieved when all of these contributors are utterly optimized, which could not be done for the presented research. Yet, this challenging SRAM case is ideal for demonstrating how the application of SMO and freeform illumination becomes increasingly beneficial when device downscaling is pursued.

5 DOE versus Flexray Source: Comparison of Patterning Results

Wafer exposures have been carried out just before and just after the installation of the FlexRay illuminator on an ASML XT:1950i. This allowed comparing the patterning behavior with a freeform DOE and the FlexRay illuminator on one particular scanner system. A more extensive benchmarking of Aerial (DOE) and FlexRay performance can be found in the Refs. 7, 9, and 10.

The use case in this investigation is the same 0.099 μm^2 SRAM contact split layer as in Sec. 3 above, exposed with freeform illumination (see Fig. 3). The sources as measured before (DOE) and after (FlexRay) the illuminator upgrade are shown in Fig. 12, as well as the respective wafer images obtained at best focus and best dose. Both for the source as the wafer image, the match between the pixelated DOE and FlexRay result is remarkably good.

Next, the wafer results are compared in a more quantitative manner. With the same metrology as above, the different

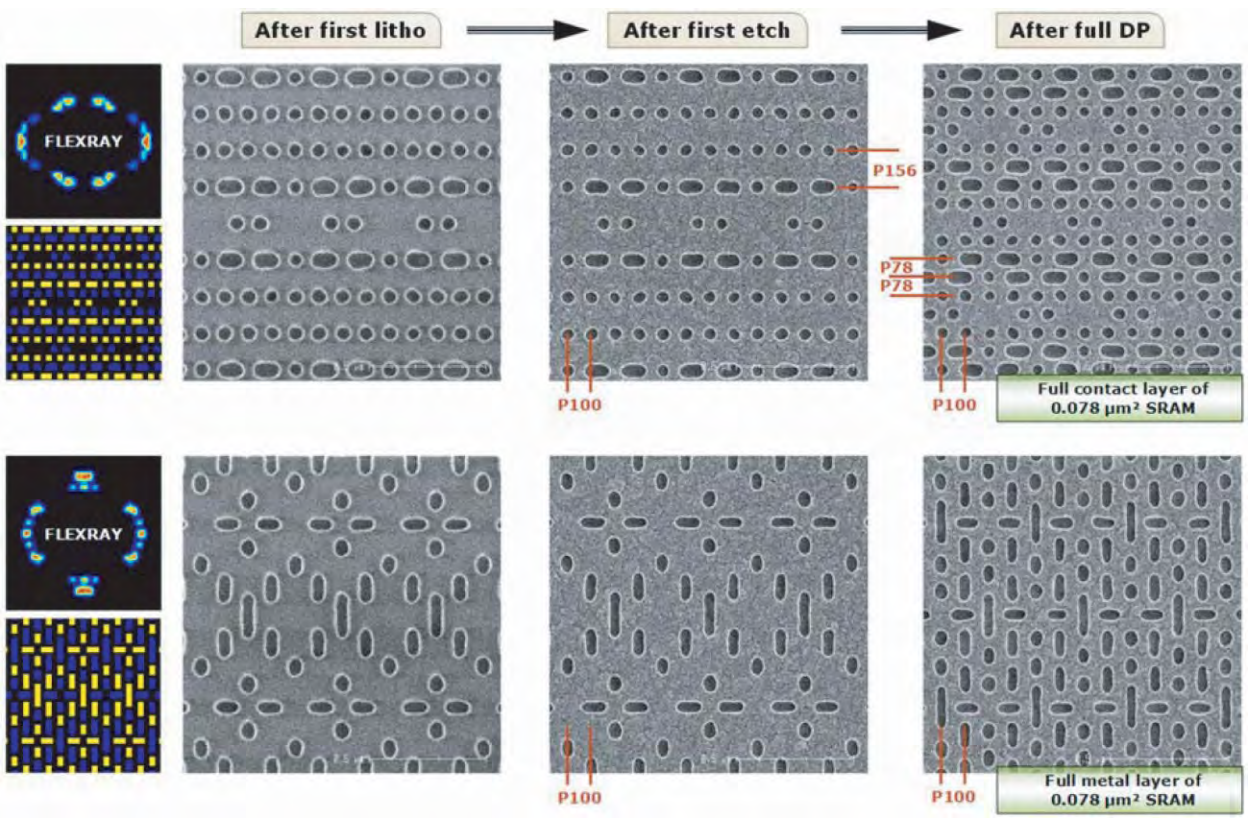

Fig. 11 Contact and metal layers of a downscaled SRAM with 0.078 μm^2 bit cell area, after first litho, etch, and after double patterning into a TiN hard mask. The exposures were done on an ASML XT:1950i with FlexRay.

Downloaded From: http://nanolithography.spiedigitallibrary.org/ on 04/08/2013 Terms of Use: http://spiedl.org/terms

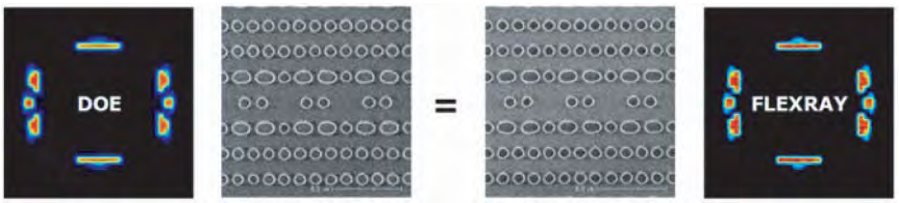

Fig. 12 Comparison of measured freeform source pupil and SEM image at best focus/dose, obtained from one and the same ASML XT:1950i before and after the upgrade from DOE to FlexRay illumination.

contact features on the DOE and FlexRay wafers from the XT:1950i are measured. (Note: these exposures were done on an XT:1900i scanner of a different generation as compared to the one used for the experiments described in Sec. 3. Moreover, the type of wafers used for the DOE – FlexRay comparison are pure Si wafers, and not oxide/TiN stack wafers as used for all the other exposures in this work. For this reason, the attentive reader may notice a small difference in process latitudes in the data of Fig. 6 versus Fig. 13.) The results are shown in Fig. 13. For all features, it can be concluded that the obtained process windows for the DOE and FlexRay sources are identical. In addition, the measured CDs at best focus and best dose were interpolated from the measured Bossung curves, and were found to be virtually equal (within the measurement accuracy).

This example demonstrates how the FlexRay upgrade of the illuminator on an existing scanner gives rise to unaltered imaging performance, which is a prerequisite for several IC manufacturers currently running production with the Aerial illuminator and considering the upgrade to FlexRay in order to increase the system's potential.

The capability to generate both traditional and fully freeform sources on demand, with virtually unlimited tuning potential, makes the FlexRay illuminator a convenient tool for both exploratory work and production, compatible with the existing nodes and ready for the coming nodes.

6 Conclusion

An experimental validation was carried out to demonstrate the benefit of freeform illumination over standard illumination. To do so, the exercise was carried out in full length, starting from an aggressive target clip matching to nowadays IC manufacturer's demands, over the source and masks calculation and manufacturing, to wafer data and double patterned result in a representative stack. To calculate the optimal source and mask combinations, ASML BRION Tachyon SMO™ was used. It was shown how a freeform DOE could be manufactured virtually perfectly on target with respect to the source calculated by the SMO engine. First, this demonstrates the state-of-the-art capabilities for freeform DOE making, and second it confirms that the Tachyon SMO correctly takes the source manufacturing constraints

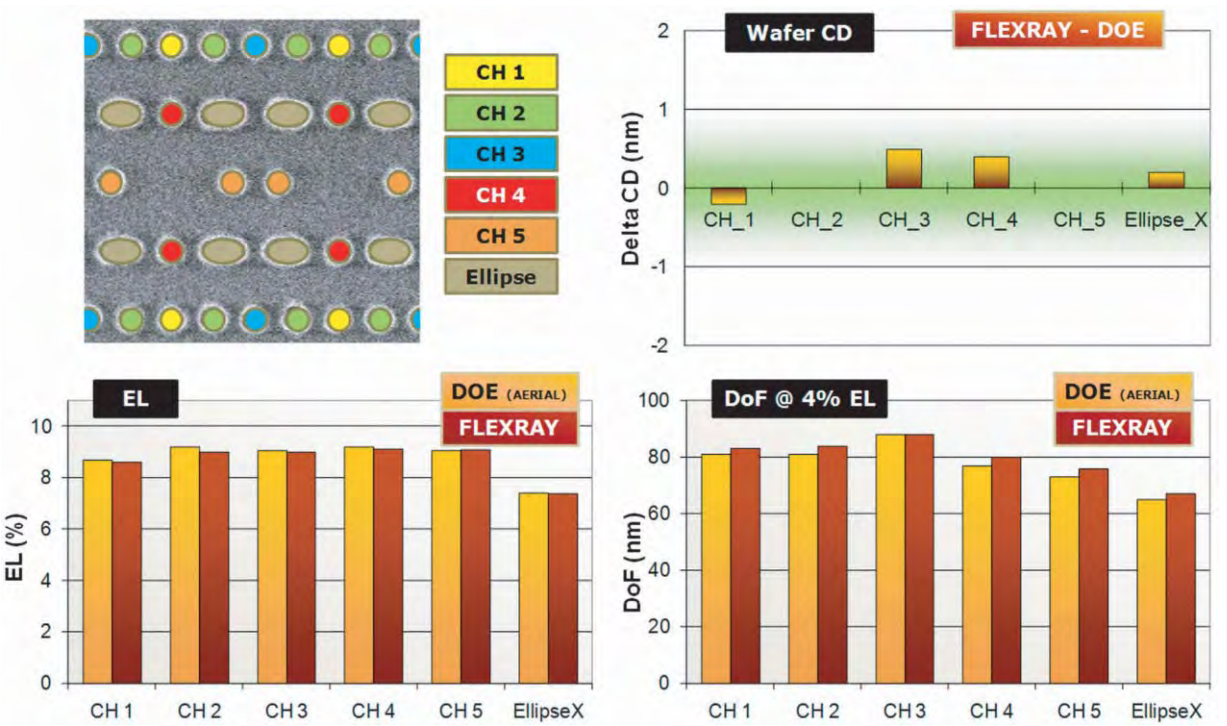

Fig. 13 Comparison of wafer CD and process window, obtained from one and the same ASML XT:1950i before and after the upgrade from DOE (Aerial) to FlexRay illumination.

Downloaded From: http://nanolithography.spiedigitallibrary.org/ on 04/08/2013 Terms of Use: http://spiedl.org/terms

into account. For the studied case of the contact layer of a 22 nm SRAM (0.099 and 0.078 μm^2 bit cell area), the wafer results clearly show the improvement in process latitudes and MEEF for freeform illumination. In particular, the greatest enhancement was found for the most difficult feature in the design. The advantage of freeform illumination was also demonstrated in CDU and no particular issues related to lens heating were found. In this way, it was demonstrated how the use of freeform illumination increases the full process yield, and thereby creates margin allowing for further device downscaling. Finally, exposures on a fully operational ASML scanner just before and just after the switch from an Aerial to FlexRay™ illuminator revealed a perfect match in the measured wafer data. The latter proves how the FlexRay option, which allows the user to instantaneously setup virtually any desired source pupil, can do so with exact match to the DOE pupil, and without change in wafer CD or loss of process latitudes. In conclusion, the paper demonstrated how the application of SMO and freeform illumination can take part in extending the applicability of ArF lithography.

Acknowledgments

The authors are very grateful for all support given to this project. In particular, P. De Bisschop, R. De Ruyter, J. Van de Kerkhove (IMEC), M. Mulder, A. Bouma, E. van der Heijden, J. Finders, S. Hansen, J.-W. Gemmink, R. Carpaij, S. Baron, M.-C. Tsai, K. Ning (ASML/ BRION), C. Hennerkes (Zeiss), J.-H. Peters (AMTC), K. Bubke (GlobalFoundries), M. Reybrouck, and S. Tarutani (FujiFilm) are acknowledged for their help, practical discussions, and organizational support.

References

1. K. Lai et al., "Experimental result and simulation analysis for the use of pixelated illumination from source mask optimization for 22nm logic lithography process," *Proc. SPIE* **7274**, 72740A (2009).
2. A. E. Rosenbluth, "Intensive optimization of masks and sources for 22nm lithography," *Proc. SPIE* **7274**, 727409 (2009).
3. L. Pang, "Source mask optimization (SMO) at full chip scale using inverse lithography technology (ILT) based on level set methods," *Proc. SPIE* **7520**, 75200X (2009).
4. S.-J. Chang, "Abbe-PCA-SMO: microlithography source and mask optimization based on Abbe-PCA," *Proc. SPIE* **7520**, 75202G (2009).
5. S. Hsu, Z. Li, L. Chen, K. Gronlund, H.-Y. Liu, and R. Socha, "Source-mask co-optimization: optimize design for imaging and impact of source complexity on lithography performance," *Proc. SPIE* **7520**, 75200D (2009).
6. S. Hsu et al., "An innovative Source-Mask co-Optimization (SMO) method for extending low k1 imaging," *Proc. SPIE* **7140**, 714010 (2008).
7. J. Zimmermann et al., "Generation of arbitrary freeform source shapes using advanced illumination systems in high-NA immersion scanners," *Proc. SPIE* **7640**, 764005 (2010).
8. J. Carriere, J. Stack, J. Childers, K. Welch, and M. D. Himel, "Advances in DOE modeling and optical performance for SMO applications in immersion lithography at the 32-nm node and beyond," *Proc. SPIE* **7640**, 764025 (2010).
9. M. Mulder et al., "Performance of a programmable illuminator for generation of freeform sources on high NA immersion systems," *Proc. SPIE* **7520**, 75200Y (2009).
10. M. Mulder et al.; "Performance of FlexRay: a fully programmable illumination system for generation of freeform sources on high-NA immersion systems," *Proc. SPIE* **7640**, 76401P (2010).
11. A. Engelen, M. Mulder, I. Bouchoms, A. Bouma, A. Ngai, M. van Veen, S. Hansen, and J. Zimmermann, "Imaging solutions for the 22nm node using 1.35NA," *Proc. SPIE* **7274**, 72741Q (2009).
12. S. Tarutani, S. Kamimura, Y. Enomoto, and K. Katou, "Resist material for negative tone development process," *Proc. SPIE* **7639**, 763904 (2010).
13. L. Van Look et al., "Printing the metal and contact layers for the 32- and 22-nm node: comparing positive and negative tone development process," *Proc. SPIE* **7640**, 764011 (2010).
14. J. Finders et al., "Litho and patterning challenges for memory and logic applications at the 22-nm node," *Proc. SPIE* **7640**, 76400C (2010).

Biographies and photographs of the authors not available.

Downloaded From: http://nanolithography.spiedigitallibrary.org/ on 04/08/2013 Terms of Use: http://spiedl.org/terms